Periplasmic Loop P2 of the MalF Subunit of the Maltose ATP Binding Cassette Transporter Is Sufficient To Bind the Maltose Binding Protein MalE[†]

Tomas Jacso,[‡] Mathias Grote,[§] Martin L. Daus,[§] Peter Schmieder,[‡] Sandro Keller,[‡] Erwin Schneider,[§] and Bernd Reif*[,‡,||]

Leibniz-Institut für Molekulare Pharmakologie (FMP), Robert-Rössle-Strasse 10, D-13125 Berlin, Germany, Institut für Biologie, AG Bakterienphysiologie, Humboldt-Universität zu Berlin, Chausseestrasse 117, D-10115 Berlin, Germany, and Charité Universitätsmedizin, D-10115 Berlin, Germany

Received July 23, 2008; Revised Manuscript Received January 16, 2009

ABSTRACT: The *Escherichia coli* maltose transporter belongs to the ATP binding cassette (ABC) transporter superfamily. Recently, the crystal structure of the full transporter $MalFGK_2$ in complex with the maltose binding protein (MBP) was determined [Oldham, M. L., et al. (2007) Crystal structure of a catalytic intermediate of the maltose transporter. *Nature 450*, 515−522]. Using liquid-state NMR, we find that the periplasmic loop P2 of MalF (MalF-P2) folds independently in solution and adopts a well-defined tertiary structure which is similar to the one found in the crystal. MalF-P2 interacts with the maltose binding protein, independent of the transmembrane region of MalF and MalG with an affinity of ∼10−20 μM, in the presence and absence of substrate. Analysis of residual dipolar coupling (RDC) experiments shows that the conformation of the two individual domains of MalF-P2 is preserved in the absence of MalE and resembles the conformation in the X-ray structure. Upon titration of MalE to MalF-P2, the two domains of MalF-P2 change their relative orientation to accommodate the ligand. In particular, a conformational change of domain 2 of MalF-P2 is induced, which is distinct from the conformation found in the X-ray structure.

ATP binding cassette (ABC)[1] transporters are ubiquitous membrane protein complexes that use the energy generated from ATP hydrolysis to transport solutes across the membrane (*1*). In bacteria, the majority of ABC transporters are importers that consist of a substrate-binding protein, two integral membrane components, and two membrane-associated ATP binding cassettes. One classical representative is the maltose transporter of *Eschericha coli*/*Salmonella* composed of the periplasmic maltose binding protein (MBP) MalE, the two integral cytoplasmic membrane proteins MalF and MalG, and two copies of the ATPase subunit MalK (*2*). In bacteria and archaea, binding proteins are the main determinants of substrate specificity. The determination of the crystal structure of the reconstituted maltose transport $MalFGK_2$ in complex with MalE has recently drawn a lot of attention to this system (*3*). There, the large periplasmic loop P2 of MalF (MalF-P2) is in contact with MalE from which maltose has already been released. In fact, MalF-P2 seems to act as a receptor which recruits MalE, and thus maltose, to the pore of the membrane protein. We are attempting to understand if this interaction occurs as well in solution. An alternative docking site might involve the periplasmic loop P3 of MalG which interacts with the maltose binding site of MalE in the X-ray structure. The question of how much MalF-P2 contributes to substrate recognition is still unresolved. Earlier genetic and biochemical investigations show that both MalF and MalG are involved in binding to the substrate-binding protein MalE (*4, 5*). It could be demonstrated that the N-terminal lobe of MalE interacts with MalG, whereas the C-terminal part of MalE is close in space to MalF. We find that MalF-P2 interacts with MalE in a manner independent of maltose. We show that MalF-P2 adopts a well-defined tertiary structure independent of other parts of the transporter.

MATERIALS AND METHODS

Plasmid Design. A DNA fragment of the MalF gene of *E. coli* encompassing codons 93−275 was amplified by polymerase chain reaction (PCR). According to the topology of MalF, this fragment covers the entire P2 loop sequence (*3, 6*). The fragment was subcloned into expression vector pET-15 (Novagen), resulting in plasmid pMG15. The plasmid integrity was verified by nucleotide sequencing. Cysteine residues replacing MalF-P2(T177), MalE(T31), and MalE-(K179) were introduced by Stratagene's Quikchange kit using plasmids pMG15 and pCB6 (*5*) as templates for *malFP2* and *malE*, respectively. The resulting plasmids were named pMM57 (MalF-T177C), pMM47 (MalE-K179C), and pMM55 (MalE-T31C).

Expression and Purification. (i) MalF-P2. Uniformly ^{15}N-labeled MalF-P2, ^{15}N- and ^{13}C-labeled MalF-P2, and ^{15}N-,

[†] This work was supported by the Leibniz-Gemeinschaft and the DFG (Grants RE1435, SCHN274, SFB 449, and SFB 740).

* To whom correspondence should be addressed. E-mail: reif@fmp-berlin.de. Phone: +49 30 94791-191. Fax: +49 30 94793-199.

[‡] Leibniz-Institut für Molekulare Pharmakologie (FMP).

[§] Humboldt-Universität zu Berlin.

[||] Charité Universitätsmedizin.

[1] Abbreviations: NMR, nuclear magnetic resonance; RDCs, residual dipolar couplings; ABC, ATP binding cassette; MBP, maltose binding protein; TMD, transmembrane domain.

10.1021/bi801376m CCC: $40.75
Published on Web 01/21/2009

^{13}C-, and ^{2}D-labeled MalF-P2 were overproduced in *E. coli* BL21 DE3 (pLysS) harboring plasmid pMG15. ^{15}N-labeled protein was amplified using $^{15}NH_4Cl$ as the sole nitrogen source. ^{13}C labeling and ^{2}H and ^{13}C labeling were achieved using [^{1}H,^{13}C]glucose and [^{2}H,^{13}C]glucose, respectively, as the carbon source. Deuterated protein was prepared using 99.9% D_2O in M9 minimal medium. The cell lysate was incubated for 4 h at 4 °C with an equilibrated nickel matrix (Ni Sepharose 6 Fast Flow, GE Healthcare). The column was washed with 25 mM imidazole to prevent unspecific binding. The protein was eluted at an imidazole concentration of 250 mM. The N-terminal His tag was cleaved off by thrombine digestion (Thrombine CleanCleave kit, Sigma, Deisenhofen, Germany). The protein solution was dialyzed and, as a final purification step, subjected to a Superdex 75 gel filtration column to remove residual imidazole, His tag fragments, and any impurities. MalF-P2 is monomeric in solution under the conditions employed in this study as shown by analytical ultracentrifugation (Supporting Information).

(ii) MalE (MBP). Polyhistidine-tagged MalE was overproduced in strain JM109 harboring plasmid pCB6 and purified as described in ref *5*.

Cross-Linking. Cross-linking experiments were performed as described previously (*7*) using Cu(1,10-phenanthroline)$_2$-SO_4 (CuPhe) to covalently link two proteins.

Sample Preparation. (i) NMR Spectroscopy. MalF-P2 samples were measured in 20 mM phosphate buffer (pH 7.4) with and without 500 μM maltose, 100 mM NaCl, 0.01% NaN_3, and 10% D_2O as the lock solvent, at protein concentrations ranging from 0.5 to 1.0 mM. Dipolar coupling measurements were carried out using liquid-crystalline Pf1 filamentous phages (purchased from Profos AG) as an alignment medium at a concentration of 7 mg/mL (residual quadrupolar coupling of $^{2}H_2O$ splitting $\sim$ 17.5 Hz), as described by Yang et al. (*8*). Titration experiments were performed using [MalF-P2]:[MalE] molar ratios of 10:1, 1:1, and 1:8, in the presence and absence of 1 mM maltose.

(ii) ITC. To prepare protein samples for ITC titration experiments, 2 mL of 1 mM solutions of MalE and MalF-P2 was dialyzed (Spectral/Por, Spectrum Laboratories Inc.) individually in 20 mM phosphate buffer [100 mM NaCl (pH 7.4)] with and without maltose (employing concentrations ranging from 500 μM to 100 mM), overnight at 7 °C with light stirring. MalE (700−800 μM) and MalF-P2 (50 μM) were filtered, degassed, and inserted into the injection syringe and calorimeter cell.

NMR Experiments and Analysis. NMR data were recorded by using Bruker 600 and 750 MHz spectrometers (Bruker Biospin, Karlsruhe, Germany), both equipped with triple-resonance cryogenic probes. For backbone and side chain assignments of MalF-P2, standard triple-resonance experiments (^{15}N HSQC-TROSY, HNCA, CBCANH, CBCA-CONH, ^{13}C TOCSY-HMQC, ^{13}C COSY-HMQC, HCCH-TOCSY, and HCCH-COSY) (*9*) were conducted, adjusting the sample temperature to 27 °C. ^{15}N T_1 and T_2 relaxation rates were determined as described in ref *10*, and the calculated overall correlation times (τ_C) were compared to tabulated values of τ_C for globular proteins of different sizes to estimate the dynamical character of MalF-P2 (*11, 12*). ^{15}N HSQC IPAP (*13*) and *J*-resolved HNCO, HNCA pulse experiments (*14*) were employed to determine the residual dipolar couplings (RDCs) ($N_iH_i^N$, $C\alpha_iC'_i$, $H\alpha_iC\alpha_i$) of MalF-P2 in its free form. After additon of MalE, $^{1}H-^{15}N$ HSQC and $^{1}H-^{15}N$ HSQC-TROSY experiments were used to measure $N_iH_i^N$ RDCs. All NMR data were processed using XWIN-NMR and Topspin (Bruker Biospin) and analyzed with CCPN (*15*). Backbone dihedral angle prediction was performed using ^{15}N, $^{13}C'$, $^{13}C\alpha$, and $^{13}C\beta$ chemical shifts of MalF-P2 after correction for ^{2}H isotopic effects (*16*). Structural restraints were generated using TALOS (*17*). The experimental residual dipolar couplings (RDCs) were correlated against amino acids N93−K275 of the crystal structure of the *E. coli* maltose transporter (Protein Data Bank entry 2R6G) (*3*), employing the molecular alignment prediction program PALES (*18*). Dipolar couplings were fitted using the best-fit module of the program. Three data sets of dipolar couplings (two data sets for free MalF-P2 and one data set in complex with MalE) were correlated to amino acids N93−K275 (full-length MalF-P2), N93−G260 (full-length MalF-P2 without the C-terminus), N93−S113 and P209−T259 (MalF-P2, domain 1), and G117−T207 (MalF-P2, domain 2) of MalF-P2 of the X-ray structure.

ITC Experiments and Analysis. High-sensitivity microcalorimetry (*19*) was performed on a VP-ITC instrument (MicroCal Software, Northampton, MA). Experiments were performed at 5 and 25 °C with MalE protein solutions in the calorimeter cell and MalF-P2 solutions in the injection syringe. The time spacings between the injections were sufficiently long to allow for complete re-equilibration (600 s). Typically, 20−40 injections were performed. Baseline subtraction and peak integration were accomplished using Origin 5.0 as described by the manufacturer (MicroCal Software). Curve fitting was performed with a nonlinear fit based on a one-site binding model. The first injection was always excluded from evaluation because it usually suffers from sample losses due to mounting of the syringe and equilibration preceding the actual titration.

Crystal Structure Analysis. Structure interpretations of the crystal structure of the maltose transporter (*3*) were done with CCP4i 1.3.20 (Computational Project, Number 4, 1994) (*20*) and PyMol (*21*). Secondary structure elements of MalF-P2 in the X-ray structure were extracted using the *dss* algorithm in PyMol. Atom−atom distance searches, between MalE and MalF-P2 in the crystal structure of the maltose transporter, were set within the range of 0.0−5.0 Å; 417 contacts shorter than 5.0 Å between MalF-P2 and MalE are found for 35 residues in the N-terminal lobe of MalE and 24 residues in MalF-P2 (Figure 6). All distances originate from heavy atoms N, C, and O.

RESULTS

Figure 1A displays a structural representation of MalF-P2 in the context of the full maltose transporter. MalF-P2 is colored red. Protein Data Bank entry 2R6G (*3*) was employed to generate the figure. To study the interactions between periplasmic loop P2 of MalF and the maltose binding protein MalE, we expressed MalF-P2 (amino acids N93−K275) (*6*) as an individual protein. We find that MalF-P2 folds independently. The $^{1}H-^{15}N$ HSQC correlation yields a well-resolved spectrum indicating that the P2 loop of MalF is well-structured (Figure 1B). Analytical ultracentrifugation shows that MalF-P2 is monomeric under the conditions employed in this study (see the Supporting Information).

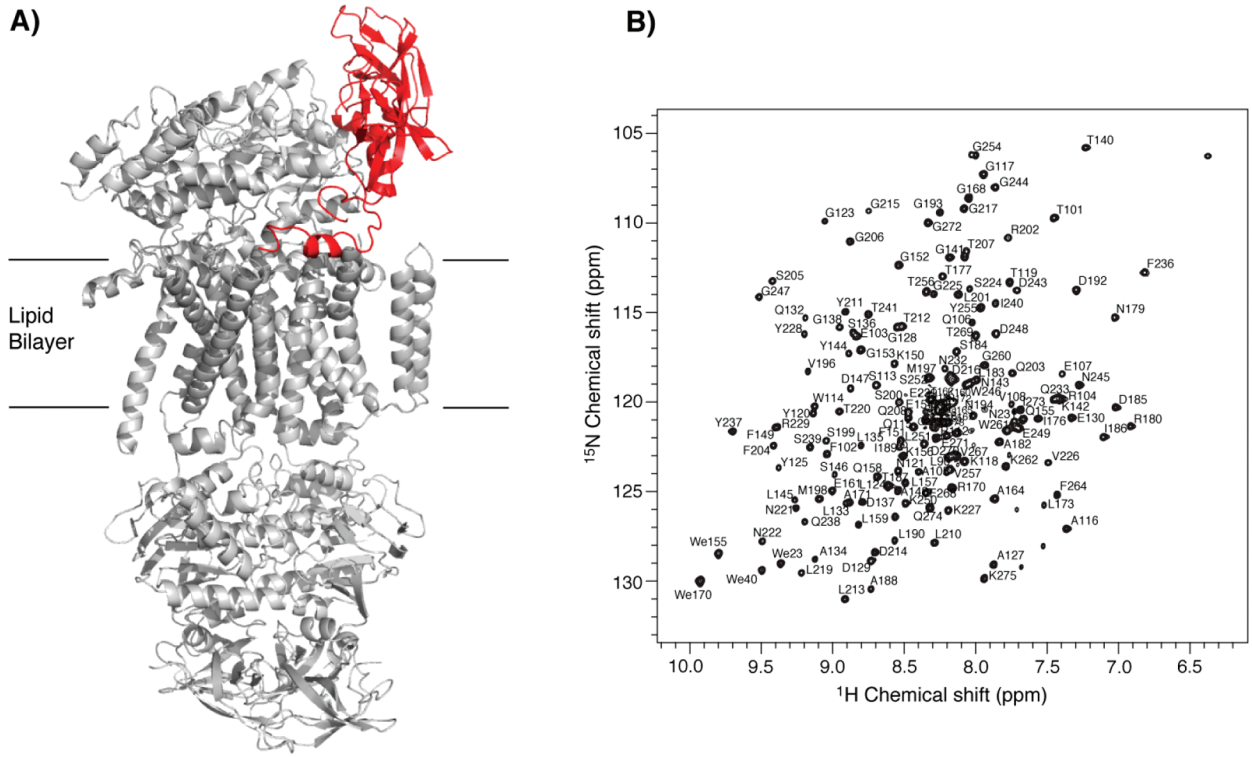

FIGURE 1: (A) MalFGK$_2$−MalE structure (Protein Data Bank entry 2R6G) system (*3*). The second periplasmic loop of MalF (MalF-P2) is colored red. (B) ^{1}H−^{15}N HSQC TROSY correlation experiment with MalF-P2. The assignments of MalF-P2 are deposited in the BMRB database, as accession code BMRB-15911 (*22*).

^{15}N T_1 and T_2 relaxation times were determined experimentally. Analysis of the relaxation rates yields an overall correlation time of the molecule (τ_C) of 8.4 ns. This correlation time is consistent with a 15 kDa protein in solution (*11, 12*).

Structural Analysis of MalF-P2 in the Crystal (X-ray) and in Solution (NMR). An analysis of the Cα/Cβ NMR chemical shifts allows us to directly assess the secondary structure elements that are adopted by MalF-P2 in solution. The assignment of NMR chemical shifts is based on CBCANH, CBCACONH, and HNCA correlation experiments performed with a ^{2}H, ^{13}C, ^{15}N isotopically enriched protein (*22*). After correction for ^{2}H secondary shifts (*16*), we can predict the preferentially assumed secondary structure elements using TALOS (*17*). Figure 2 represents a comparison of the secondary structure elements found in the X-ray structure and by NMR. The predicted secondary structure matches the crystal structure very well with the exception of the amphipathic α-helix at the C-terminus of MalF-P2. We find small differences between the X-ray and NMR secondary structure prediction. TALOS requires a minimum of three consecutive amino acids displaying the same secondary structure propensities for assignment of a secondary structure element. Therefore, β-strands β1 and β8, which have a length of two residues only in the X-ray structure, are missing. In addition, strands β5 (residues 155−158) and β11 (residues 225−230) are absent in the NMR analysis as a complete set of Cα/Cβ chemical shifts for residues 154 and 229, respectively. In the X-ray structure, the side chains of aromatic residues W260, F263, and F267 are oriented in the direction of the lipid bilayer, supporting the idea that the α-helix (residues 260−269) serves as an anchor to attach MalF-P2 to the lipid bilayer. We find that the C-terminus of MalF-P2 has a decreased number of secondary structure elements in solution

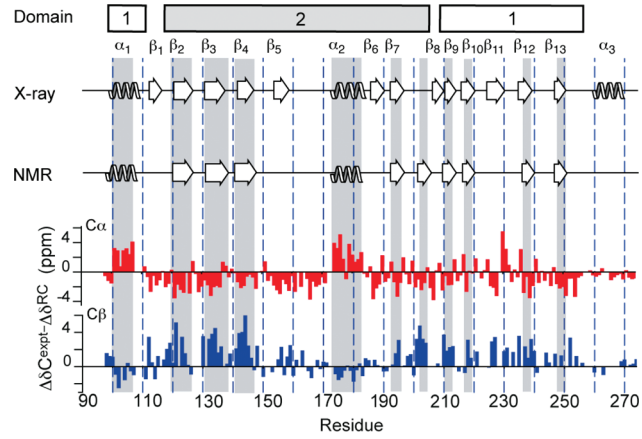

FIGURE 2: Comparison of adopted secondary structure elements of MalF-P2 in the MalFGK$_2$−MalE X-ray structure (*3*) and in the separately expressed MalF-P2 loop as predicted by NMR chemical shift analysis. The indicated secondary structure is based on the Cα/Cβ NMR chemical shift data employing TALOS (*17*). The bottom of the figure represents differences between random coil (RC) and experimental (expt) chemical shifts for Cα and Cβ as a function of the primary sequence in MalF-P2. Secondary structure elements as predicted by TALOS are highlighted in gray. MalF-P2 folds into two individual domains (domain 1, residues 91−113 and 209−259; domain 2, residues 117−207) which are connected via β-strands β1 and β8.

compared to the X-ray structure. It is likely that interactions with MalF and MalG are required to induce formation of those secondary structure elements.

To probe structural differences of MalF-P2 in solution and in the crystalline state, we performed residual dipolar coupling (RDC) measurements (*23, 24*). Upon alignment, the anisotropic dipolar coupling is not averaged any longer. The residual dipolar component in the doublet splitting reflects directly the orientation of a particular bond vector

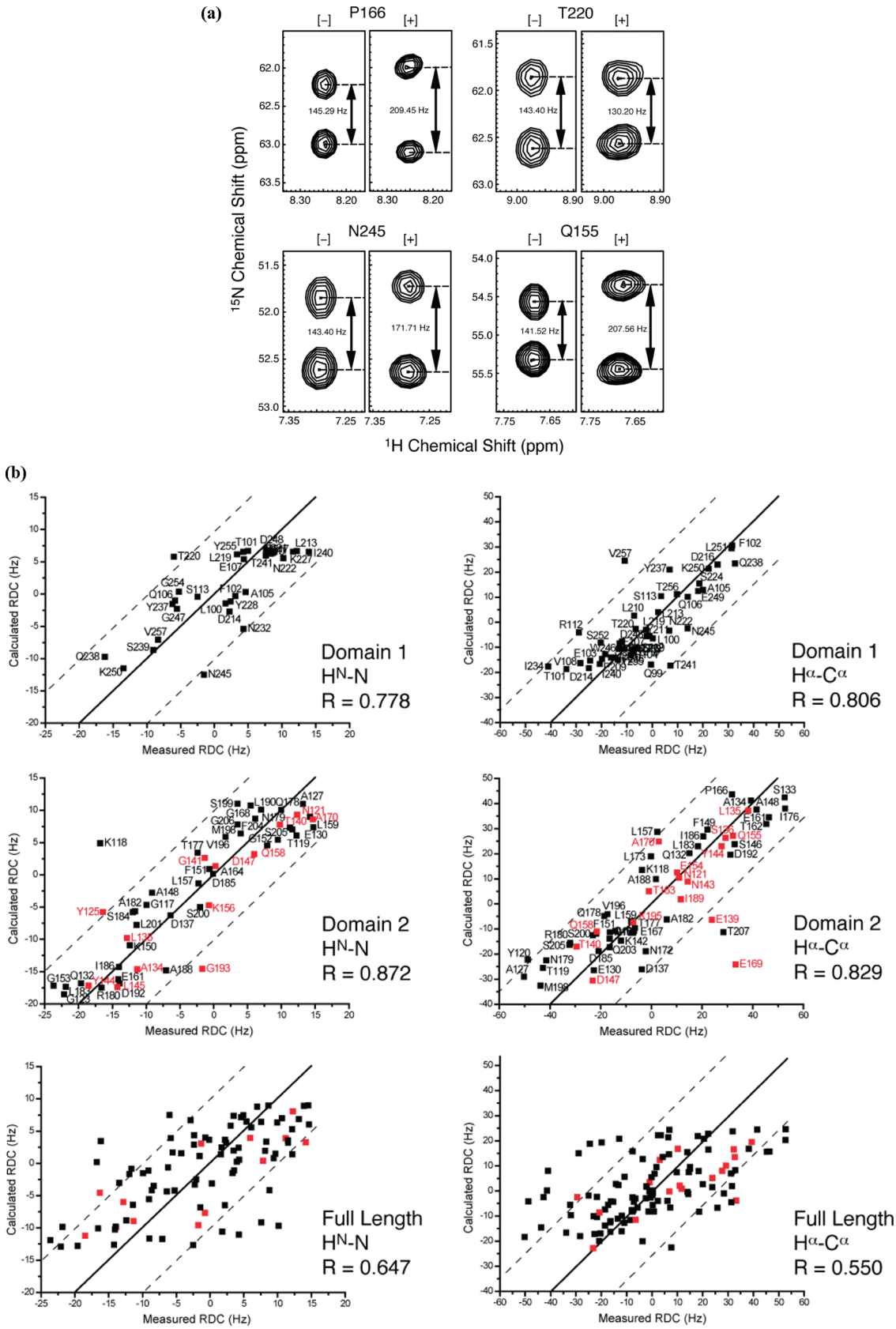

FIGURE 3: (a) Hα−Cα residual dipolar couplings (RDCs) for selected residues in MalF-P2. Pf1 phages (7 mg/mL yielding a residual quadrupolar coupling of the D_2O resonance on the order of 17.5 Hz) were used as an alignment medium (*25, 26*). [−] and [+] indicate that the respective spectrum was recorded in the absence and presence of alignment medium, respectively. All spectra were recorded without maltose in the sample buffer. (b) Predicted RDC values vs experimental RDCs of MalF-P2 using PALES (*18*). Using H^N−N and Cα−Hα RDC data, domain 1 (residues 91−113 and 209−259) correlates with an average *R* value of 0.79 and domain 2 (residues 117−207) with an *R* value of 0.85. All experimental RDC values could be fit to the full structure of the MalF-P2 loop, yielding an average *R* value of 0.59. Residues which are colored red are involved in crystal contacts with a MalK molecule in the symmetry-related unit cell (see the Supporting Information).

Table 1: Correlation Coefficients Calculated by Fitting Experimental RDC Values to the X-ray Structure of the MalFGK$_2$•E Complex Using PALES (*18*)[a]

		domain 1	domain 2	domain 1 and domain 2	domain 1, domain 2, and C-terminus
		Free MalF-P2			
H^N-H	all amino acids	0.78	0.87	0.68	0.65
	excluding crystal contacts	−	0.87	0.66	0.62
Hα−Cα	all amino acids	0.81	0.83	0.58	0.55
	excluding crystal contacts	−	0.88	0.56	0.56
		MalF-P2 and MalE			
H^N-H	all amino acids	0.90	0.52	0.64	0.64
	excluding crystal contacts	−	0.58	0.70	0.69

[a] High correlation coefficients indicate that the conformations in the crystal and in solution are comparable. Domain 1 consists of residues 91−113 and 209−259. Domain 2 consists of residues 117−207. Full-length MalF-P2 consists of residues 93−275. Full-length MalF-P2 without the C-terminus consists of residues 93−260.

with respect to an alignment tensor that is determined by the shape of the molecule. Knowing the structure of the protein allows a back-calculation of RDCs and yields a set of theoretically predicted residual dipolar couplings (*18*). Figure 3a represents spectra for four residues extracted from a *J*-resolved three-dimensional HNCA experiment that was recorded without scalar decoupling in the ^{13}C evolution period. H^N-N and Hα−Cα residual dipolar couplings were fitted subsequently against the X-ray structure of MalF-P2. A correlation of those back-calculated RDCs and the experimental RDCs is shown in Figure 3b. A fairly good fit is obtained for the two individual domains alone. For domain 1, we determine a correlation coefficients (R) of 0.78 and 0.81 for H^N-N and Hα−Cα couplings, respectively. Similarly, we obtain a correlation coefficients (R) of 0.83 and 0.87 for H^N-N and Hα−Cα couplings, respectively, for domain 2. A better fit of the correlation of the individual domains and the complete P2 loop of MalF might be achievable for a higher-resolution X-ray structure. The X-ray structure of the maltose transporter (*3*) has a resolution of ~3 Å (root-mean-square deviation) which leaves some uncertainties concerning local structural fluctuations. No correlation is observed if all residues of the P2 loop of MalF are subjected to the fitting procedure (correlation coefficient $R = 0.65$ and 0.55 for H^N-N and Hα−Cα couplings, respectively). The fit improves only marginally when the C-terminus (residues 260−275) containing the amphipathic helix is taken out of the fit. The correlation coefficient improves then to 0.68 and 0.58 for H^N-N and Hα−Cα couplings, respectively. All correlation coefficients are summarized in Table 1. The fact that predicted and experimental RDCs match for the two domains indicates that the overall structure of the individual domains is preserved, but the relative orientation of the two domains of MalF-P2 is different in the crystal and in solution. This may be expected as the relative orientation of the two domains of MalF-P2 might change upon binding to MalE.

Interactions between MalF-P2 and MalE. To find out if and to what extent MalE can interact with the isolated P2 loop of MalF, we carried out isothermal titration calorimetry (ITC) experiments. Figure 4 shows that MalE and MalF-P2

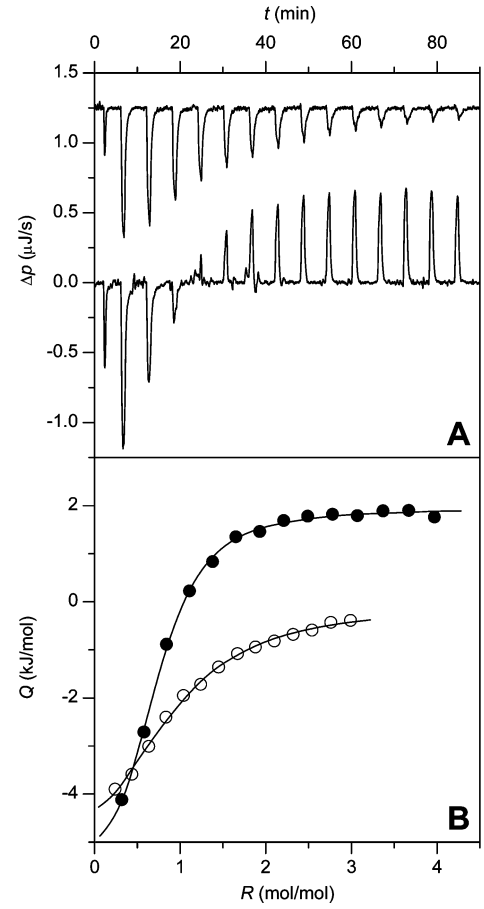

FIGURE 4: Isothermal titration calorimetry (ITC) curves obtained by titrating MalF-P2 with MalE. (A) Differential heating power, Δp, vs time t. ITC data were recorded at 5 °C in the absence (top) and presence (bottom) of maltose. One 5 μL and 14 20 μL aliquots of a concentrated MalE solution (667 μM in the absence of maltose, 885 μM in the presence of maltose) were injected into a 50 μM MalF-P2 solution in the absence (top trace) or presence (bottom trace) of 100 mM maltose. For the sake of clarity, the ITC curve obtained without maltose (top trace) was arbitrarily shifted along the ordinate by 1.25 μJ/s. Constant endothermic peaks at the end of the titration with maltose (bottom trace) were due to dilution effects (most likely originating from slight differences in maltose concentration) and were also observed in control experiments in which MalE was injected into dialysis buffer containing 100 mM maltose but no P2 (data not shown). (B) Integrated and normalized heats of reaction, Q, vs MalE/P2 molar ratio, R. Fits (solid lines) to experimental data obtained in the absence (empty symbols) or presence (filled symbols) of 100 mM maltose yielded the following thermodynamic parameters characterizing the MalF-P2 interactions: $K_D = 22$ μM, $\Delta G° = -24.9$ kJ/mol, $\Delta H° = -6.2$ kJ/mol, and $T\Delta S° = 18.6$ kJ/mol in the absence of maltose; $K_D = 7.4$ μM, $\Delta G° = -27.3$ kJ/mol, $\Delta H° = -8.5$ kJ/mol, and $T\Delta S° = 18.8$ kJ/mol in the presence of 100 mM maltose. Initial 5 μL injections were excluded from the fitting procedure.

interact, even in the absence of other periplasmic loops of MalF and those of MalG. Assuming a 1:1 stoichiometry, fitting of the data yielded a dissociation constant (K_D) on the order of 10−20 μM, independent of the presence of maltose.

Binding of MalE to MalF-P2 in the absence of maltose ($K_D \approx 22$ μM) is only marginally weaker than in its presence ($K_D \approx 7.4$ μM). The endothermic peaks at the end of the titration performed in the presence of maltose are due to the heat of dilution. To confirm the interaction of purified MalF-P2 and MalE, we performed cross-linking experiments. A variant of MalF-P2 containing a mutation in domain 2

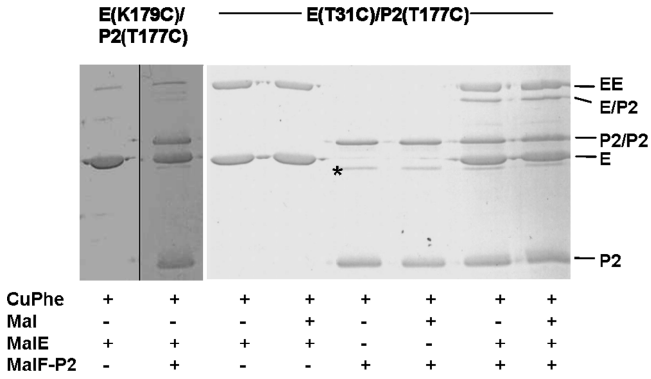

FIGURE 5: Site-specific CuPhe-induced cross-linking of the purified MalF P2 loop carrying a cysteine at position 177 with MalE(T31C) and MalE(K179C). MalF-P2 (2.5 μM) was incubated with the MalE variants (2.5 μM) and CuPhe in the absence or presence of maltose. The band marked with an asterisk is an impurity and is copurified only with the monocysteine variant of MalF-P2.

(T177C) was incubated with MalE(T31C) at a 1:1 molar ratio in the presence of CuPhe and subsequently analyzed for disulfide bond formation by SDS−PAGE. In the crystal structure, both residues are 5 Å apart and thus should readily form a disulfide bond. In fact, besides monomers and homodimers of both proteins, an additional band, comprising MalE and MalF-P2, could be observed (Figure 5) and verified by immunoblotting (data not shown). The product was found independent of the presence or absence of maltose, thereby confirming the results presented above. In contrast, only a faint band migrating at the size of a MalE-P2 cross-link could be detected when MalF-P2(T177C) was incubated with CuPhe in the presence of the MalE variant K179C (Figure 5). This residue is located in the hinge region of MalE and, according to the crystal structure, not within immediate cross-linking distance of MalF-P2(T177C). This result underscores the specificity of the MalF-P2−MalE interaction.

Additionally, the interaction between MalF-P2 and MalE was followed with site-specific resolution using solution-state NMR (Figure 6). We find that specific resonances display decreased intensities or are shifted if MalE is added to a solution of ^{15}N isotopically enriched MalF-P2. Spectra in the presence and absence of MalE were recorded under identical conditions (same buffer, without maltose). Similar chemical shift perturbations are observed in the presence of maltose. This behavior is expected as the dissociation constant of the binding is in the intermediate micromolar range. In case of strong binding, two separate sets of resonances are expected, reflecting the different chemical environment of bound and free MalF-P2. In the weak-binding limit, a continuous change in the ^{1}H−^{15}N chemical shifts of MalF-P2 as a function of the concentration of MalE would yield the dissociation constant of the interaction. In the case of intermediate binding, line broadening for those residues interacting with MalE occurs. At a MalF-P2:MalE molar ratio of 10:1, small perturbations of the chemical shifts are detected. Already at this low concentration of MalE, we find slightly reduced intensities of the MalF-P2 resonances. At a 1:1 molar ratio, the intensity of a large number of resonances is drastically reduced as a consequence of the interaction with MalE. Residues belonging to the C-terminal part and to the external loops of MalF-P2 remain largely unaffected by the binding process.

Strong interactions between MalF-P2 and MalE are also observed in the crystal structure of the MalFGK$_2$-E maltose transporter. Figure 7A summarizes the structural contacts observed in the crystal structure and the ones found in the NMR experiment. In the analysis of the X-ray contacts, all residues for which a heavy atom of MalF-P2 is within 5 Å of a heavy atom of MalE are taken into account. Residues which were selected as NMR interaction sites show a chemical shift change $\{[\delta\Delta(^{1}H) + \delta\Delta(^{15}N)/5]^{1/2}\}$ larger than 0.03 ppm, which is equivalent to a ^{1}H shift change of 22.5 Hz at 750 MHz. Residues which are involved in the interaction are located in secondary structure elements α1 and β1 (residues 100−110) and α2 and β6 (residues 175−191), as well as in both linker region elements β1 and β8 which connect domains 1 and 2, including residues 112−116 and 200−208, respectively.

Figure 7B focuses on MalF-P2 (ribbon) and MalE (surface representation). For MalF-P2 residues which are colored orange and red, we find significant chemical shift perturbations indicating an involvement of those residues in binding to MalE. For residues that are colored blue, chemical shifts are unaffected upon addition of MalE. To probe if MalF-P2 is structurally reorganized upon binding to MalE, we repeated the RDC experiments in the presence of MalE. Figure 8 shows a correlation between experimental and theoretical RDC couplings for MalF-P2. The theoretical RDC values are again obtained by back-calculation from the X-ray structure of the maltose transporter using PALES (*18*). The correlation coefficient for domain 1 remains high, indicating that its structure is not perturbed upon addition of MalE. On the other hand, the correlation coefficient for domain 2 decreases significantly. This implies that the structure of domain 2 is different from the structure of domain 2 in the crystal. The overall correlation coefficient remains small (R = 0.64 for all amino acids, and R = 0.64 for full-length MalF-P2 without the C-terminal residues). Residues which are colored red (domain 2) are involved in crystal contacts with a MalK molecule in the symmetry-related unit cell in the X-ray structure.

DISCUSSION

We demonstrate in this work that the second periplasmic loop, P2, of MalF adopts a well-defined structure if over-produced individually and is not unfolded in solution (Figures 1 and 2). In that sense, MalF-P2 can be regarded as a receptor that recognizes MalE. The exceptional length of the second periplasmic loop in MalF is a particular property of enterobacteria (*28*). Deletion of this region impairs maltose transport. So far, however, it is not understood why enterobacteria require the extension of the loop. Given the fact that MalF-P2 has no stabilizing contacts to any protein component other than MalE in the X-ray structure of the maltose transporter, we can assume that the isolated MalF-P2 is a good model for studying the interactions between the maltose transporter and MalE. Analysis of RDC data shows that the structure of the two subdomains of MalF-P2 is similar in the crystal and in solution in the absence of MalE (Figure 3a,b). The relative orientation of the two domains of MalF-P2 is, however, different (Figure 3c). In NMR relaxation experiments, we find a correlation time for molecular tumbling (τ_C) of 8.4 ns. At this temperature and

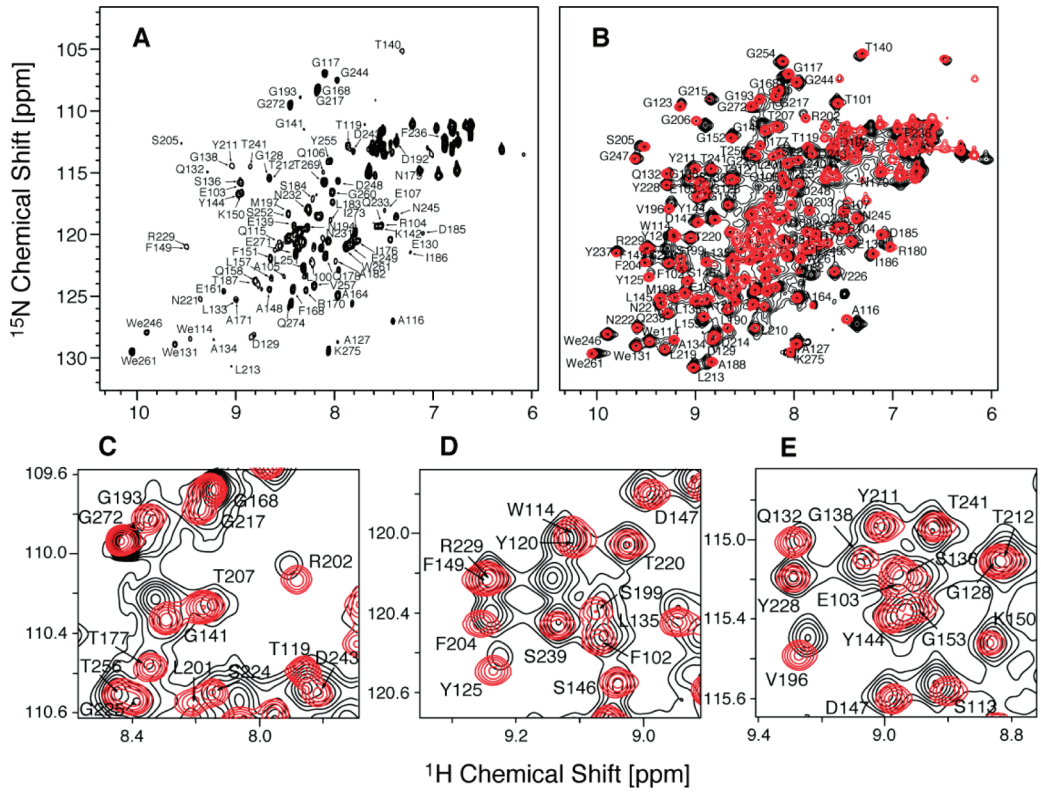

FIGURE 6: (A) ^{1}H−^{15}N HSQC titration spectra of ^{15}N isotopically enriched MalF-P2 with MalE (1:1 molar ratio). (B) Superposition of MalF-P2 in the absence (red) and presence (black) of unlabeled MalE. In contrast to panel A, panel B is represented at lower contour levels. Panels C−E focus on particular spectral regions of the spectra represented in panel B.

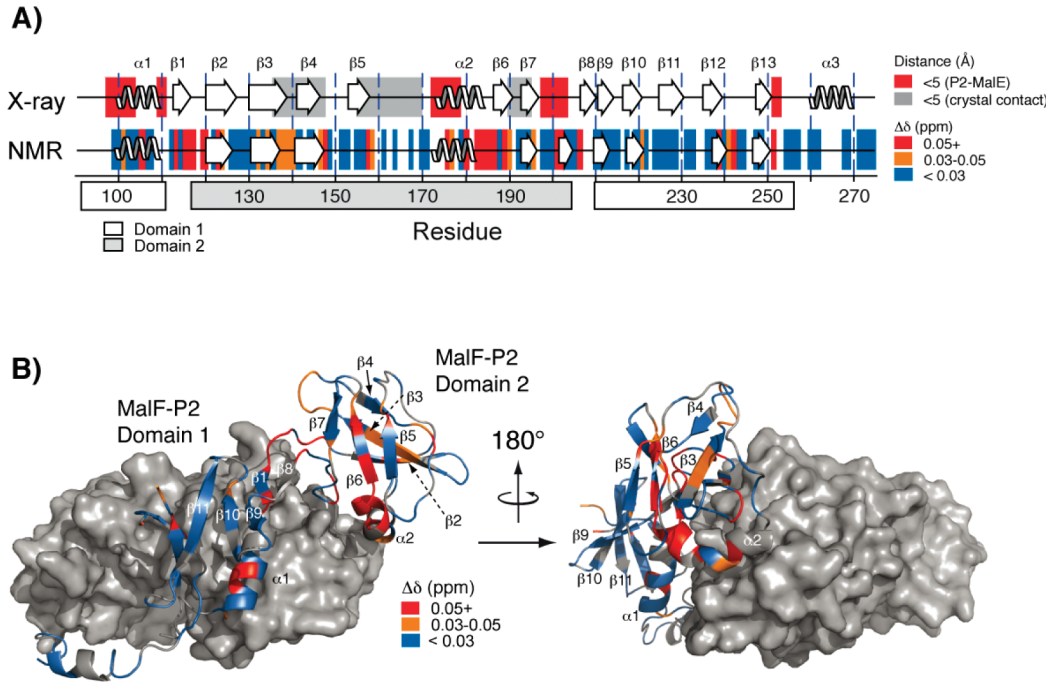

FIGURE 7: (A) Interactions between MalF-P2 and MalE, found in the crystal structure and as deduced from NMR chemical shift perturbations. In the analysis of the X-ray contacts, all residues in which a heavy atom of MalF-P2 is within 5 Å of a heavy atom of MalE (marked as red boxes) or MalK (marked as gray boxes) are taken into account. The analysis was carried out using CCP4i 1.3.20 (*27*). Sites of interaction between MalF-P2 and MalE are color-coded according to the size of the perturbation. (B) Structural representation of the residues of MalF-P2 which are experiencing chemical shift changes in the NMR experiment. MalE is drawn in surface representation.

protein concentration, this value of τ_C fits to a protein with a molecular mass of ~15 kDa. We explain this smaller than expected correlation time of the protein by assuming that the two domains of MalF-P2 can tumble independently of each other and hence have a lower τ_C than one would have anticipated for a globular protein.

Merino et al. predicted that both conformations of MalE interact with the transporter (*29*). The authors showed that

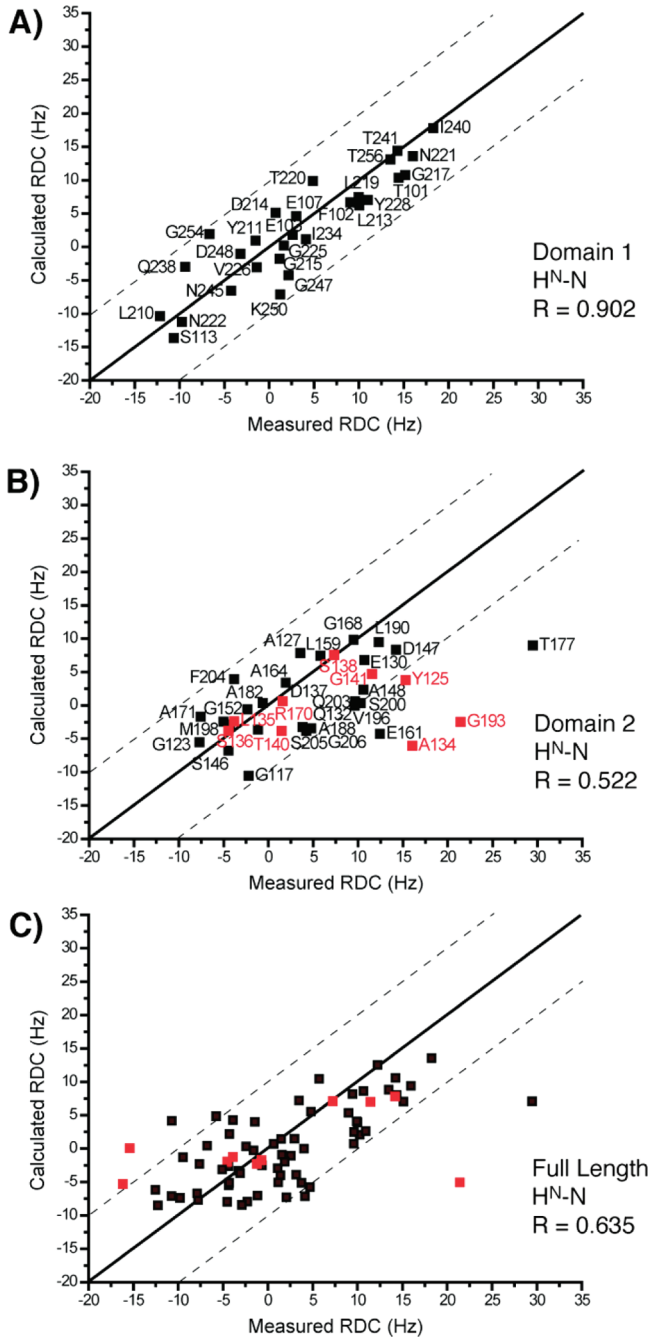

FIGURE 8: Experimental vs predicted RDC values for MalF-P2 in the presence of the maltose binding protein MalE. The theoretical RDC values are calculated from the X-ray structure using PALES (*18*). (A) RDC data fitted to domain 1 ($R = 0.90$), domain 2 ($R = 0.522$), and full-length MalF-P2 ($R = 0.64$) are represented in panels A−C, respectively. A lower correlation coefficient in the presence of MalE suggests that the conformations of domain 2 of MalF-P2 in the crystal structure and in solution are different. Residues which are colored red are involved in crystal contacts with a MalK molecule in the symmetry-related unit cell (see the Supporting Information).

unliganded MalE competes with liganded MalE in transport assays, and by fitting their data to theoretical equations, they concluded that maltose-free and maltose-bound MalE interact with the transporter with similar affinity. Both forms of the binding protein have access to the membrane components. Recent cross-linking experiments demonstrating the proximity of MalE(G13) to Pro78 in the first periplasmic loop of MalG in the presence and absence of maltose are consistent with this notion (*5*). We find that MalF-P2 specifically binds to the maltose binding protein MalE in the presence and absence of substrate with similar affinity, even in the absence of MalG and the remaining part of MalF (Figure 4). The binding affinity is on the order of 10−20 μM as determined by ITC experiments. From a structural point of view, it might be expected that the interaction between MalF-P2 and MalE is to first order independent of maltose as MalF-P2 binds to only one of the two domains of MalE. Our data are corroborated by the finding that the isolated P2 loop carrying a cysteine residue at position 177 cross-links to MalE(T31C) in the absence or presence of maltose (Figure 5). Previous biochemical experiments revealed that a MalE concentration of 25−100 μM is required to maintain half-maximal transport rates (*30, 31*). This is in agreement with EPR studies in which 60% of MalE was bound to $MalFGK_2$ at protein concentrations of 50−100 μM (*32*). Together, our findings are consistent with cross-linking data, demonstrating MalE−MalF-P2 interaction throughout the transport cycle in the context of the assembled $MalFGK_2$ complex (*33*).

Upon titration of MalE with MalF-P2, most of the NMR resonances show decreased intensities and a specific subset displays significant chemical shift changes (Figure 6), indicating that the amino acids associated with these resonances are involved in MalE binding. An interaction of MalE with the integral membrane components MalF and MalG was observed previously in the crystal structure of the catalytic intermediate state of the maltose transporter (*3*), in which the N-terminal lobe of MalE interacts with MalF (MalF-P2). The C-terminal lobe of MalE binds mostly to periplasmic loop P3 of MalG. From the NMR titration experiments, we find that the amino acids that are involved in the interaction between MalF-P2 and MalE are localized in domain 1, containing secondary structure elements α1 and β1 (residues 100−110), in domain 2 α2 and β6 (residues 175−191), and both linker regions β1 and β8 which connect domains 1 and 2, including residues 112−116 and 200−208, respectively. This is in agreement with the X-ray structure in which a similar interaction interface is found (Figure 7). The assumption that the $MalFGK_2$ complex must be able to attain at least two different conformations in its interaction with MalE, only one of which is able to trigger ATP hydrolysis by MalK (*2, 34*), is confirmed by EPR data (*32, 35*). Davidson and co-workers found that there was no change in affinity of MalE for $MalFGK_2$ in its substrate-free or substrate-bound form. This is in agreement with our ITC binding data which show that MalF-P2 interacts with MalE similarly in the presence and absence of substrate.

The fitting of H^N−N residual dipolar couplings of MalF-P2 bound to MalE yields the correlation coefficients (R) of 0.90 for domain 1, 0.52 for domain 2, and 0.64 for all residues of MalF-P2 (Figure 8). The correlation coefficient is invariant to a truncation of the C-terminus in the analysis ($R = 0.64$). All correlation coefficients determined for free MalF-P2 and MalF-P2 after addition of MalE are summarized in Table 1. In the bound state, the high correlation coefficient which is observed for domain 1 indicates that the overall structure of this domain is comparable to its structure in the unbound state. Most of the outliers in the correlation plot belong to regions of MalF-P2 at the surface of the structure, predominantly in domain 2 of MalF-P2. There, the conformation might be

perturbed due to crystal packing effects and/or dynamic effects. Indeed, we find a number of contacts between domain 2 of MalF-P2 and the MalK subunits of the symmetry-related maltose transporter in the crystal (see the Supporting Information). These residues are colored red in Figure 8. Crystal contacts might induce local structural perturbations which in turn affect the local conformation of the protein in domain 2. Apparently, domain 2 of MalF-P2 interacts preferably with a MalK molecule in a symmetry-related unit cell, such that the X-ray structure of domain 2 of MalF-P2 resembles more the structure in the unbound state.

To summarize, we find that individually expressed MalF-P2 represents a well-folded membrane protein receptor to which the maltose binding protein MalE is bound in the presence and absence of maltose. The structures of the two individual domains of MalF-P2 in the absence of MalE are comparable to the conformation found in the X-ray structure. Upon titration of MalE with MalF-P2, the two domains of MalF-P2 change their relative orientation to accommodate the ligand. Under these conditions, a conformational change of domain 2 of MalF-P2 is induced, resulting in a structure which is distinct from the conformation found in the X-ray structure. We assume that crystal contacts between MalF-P2 and MalK are the reason for differences in conformation observed in the crystal and in solution.

ACKNOWLEDGMENT

We thank Dr. Katja Faelber for assistance in the analysis of crystallographic data.

SUPPORTING INFORMATION AVAILABLE

NMR titration plots, analytical ultracentrifugation data for MalF-P2, structural representation of crystallographic contacts between maltose transporters in symmetry-related unit cells (Protein Data Bank entry 2R6G), and H^N-N and $H\alpha-C\alpha$ RDC values for MalF-P2 in the presence and absence of MalE. This material is available free of charge via the Internet at http://pubs.acs.org.

REFERENCES

1. Higgins, C. F. (1992) ABC Transporters: From Microorganisms to Man. *Annu. Rev. Cell Biol. 8*, 67–113.
2. Boos, W., and Lucht, J. M. (1996) *Periplasmic binding protein-dependant ABC transporters in E. coli and Salmonella typhimurium: Cellular and molecular biology* (Neidhardt, F. C., Curtiss, R., Ingraham, J. L., Lin, E. C. C., Low, K. B., and Magasanik, B., Eds.) pp 1175−1209, American Society for Microbiology Press, Washington, DC.
3. Oldham, M. L., Khare, D., Quiocho, F. A., Davidson, A. L., and Chen, J. (2007) Crystal structure of a catalytic intermediate of the maltose transporter. *Nature 450*, 515–522.
4. Hor, L. I., and Shuman, H. A. (1993) Genetic-analysis of periplasmic binding-protein dependent transport in *Escherichia Coli*: Each lobe of maltose-binding protein interacts with a different subunit of the $MalFGK_2$ membrane-transport complex. *J. Mol. Biol. 233*, 659–670.
5. Daus, M. L., Berendt, S., Wuttge, S., and Schneider, E. (2007) Maltose binding protein (MalE) interacts with periplasmic loops P2 and P1 respectively of the MalFG subunits of the maltose ATP binding cassette transporter ($MalFGK_2$) from *Escherichia coli*/*Salmonella* during the transport cycle. *Mol. Microbiol. 66*, 1107–1122.
6. Froshauer, S., Green, G. N., Boyd, D., McGovern, K., and Beckwith, J. (1988) Genetic Analysis of the Membrane Insertion and Topology of MalF, a Cytoplasmic Membrane Protein of *Escherichia coli*. *J. Mol. Biol. 200*, 501–511.
7. Daus, M. L., Grote, M., Müller, P., Doebber, M., Herrmann, A., Steinhof, H.-J., Dassa, E., and Schneider, E. (2007) ATP-driven MalK dimer closure and re-opening and conformational changes of the 'EAA' motifs are crucial for function of the maltose ATP-binding cassette transporter (MalFGK2). *J. Biol. Chem. 282*, 22387–22369.
8. Yang, D., Venters, R. A., Mueller, G. A., Choy, W. Y., and Kay, L. E. (1999) TROSY-based HNCO pulse sequence for the measurement of ^1HN-^{15}N, ^{15}N-^{13}CO, ^1HN-^{13}CO, ^{13}CO-^{13}C and ^1HN-^{13}C dipolar couplings in ^{15}N, ^{13}C, ^2H labeled proteins. *J. Biomol. NMR 14*, 333–343.
9. Sattler, M., Schleucher, J., and Griesinger, C. (1999) Heteronuclear multidimensional NMR experiments for the structure determination of proteins in solution employing pulsed field gradients. *Prog. NMR Spectrosc. 34*, 93–158.
10. Cavanagh, J., Fairbrother, W. J., Palmer, A. G., and Skelton, N. J. (1996) *Protein NMR Spectroscopy: Principles and Practice*, Academic Press, San Diego.
11. Gryk, M. R., Abseher, R., Simon, B., Nilges, M., and Oschkinat, H. (1988) Heteronuclear relaxation study of the PH domain of β-spectrin: Restriction of loop motions upon binding inositol trisphosphate. *J. Mol. Biol. 280*, 879–896.
12. Dayie, K. T., Wagner, G., and Lefèvre, J. F. (1996) Theory and Practice of Nuclear Spin Relaxation in Proteins. *Annu. Rev. Phys. Chem. 47*, 243–282.
13. Ottiger, M., Delaglio, F., and Bax, A. (1998) Measurement of J and dipolar couplings from simplified two-dimensional NMR spectra. *J. Magn. Reson. 131*, 373–378.
14. Bax, A., Kontaxis, G., and Tjandra, N. (2001) Dipolar couplings in macromolecular structure determination. *Methods Enzymol. 339*, 127–174.
15. Vranken, W. F., Boucher, W., Stevens, T. J., Pajon, R. F. A., Llinas, M. L., Ulrich, E., Markley, J. L., Ionides, J., and Laue, E. D. (2005) The CCPN Data Model for NMR Spectroscopy: Development of a Software Pipeline. *Proteins 59*, 687–696.
16. Venters, R. A., Farmer, B. T., Fierke, C. A., and Spicer, L. D. (1996) Characterizing the use of perdeuteration in NMR studies of large proteins C-13, N-15 and H-1 assignments of human carbonic anhydrase II. *J. Mol. Biol. 264*, 1101–1116.
17. Cornilescu, G., Delaglio, F., and Bax, A. (1999) Protein backbone angle restraints from searching a database for chemical shift and sequence homology. *J. Biomol. NMR 13*, 289–302.
18. Zweckstetter, M., and Bax, A. (2000) Prediction of Sterically Induced Alignment in a Dilute Liquid Crystalline Phase: Aid to Protein Structure Determination by NMR. *J. Am. Chem. Soc. 122*, 3791–3792.
19. Wiseman, T., Williston, S., Brandts, J. F., and Lin, L.-N. (1989) Rapid measurement of binding constants and heats of binding using a new titration calorimeter. *Anal. Biochem. 179*, 131–137.
20. Navaza, J. (1994) The CCP4 Suite: Programs for Protein Crystallography. *Acta Crystallogr. A50*, 157–163.
21. DeLano, W. L. (2002) PyMol, DeLano Scientific, San Carlos, CA.
22. Jacso, T., Grote, M., Schmieder, P., Schneider, E., and Reif, B. (2008) NMR assignments of the periplasmic loop P2 of the MalF subunit of the maltose ATP binding cassette transporter. *Biomol. NMR Assign.* doi: 10.1007/s12104-008-9131-7.
23. Tjandra, N., and Bax, A. (1997) Direct Measurement of Distances and Angles in Biomolecules by NMR in a Dilute Liquid Crystalline Medium. *Science 278*, 1111–1114.
24. Prestegard, J. H., Al-Hashimi, H. M., and Tolman, J. R. (2000) NMR structures of biomolecules using field oriented media and residual dipolar couplings. *Q. Rev. Biophys. 33*, 371–424.
25. Hansen, M. R., Mueller, L., and Pardi, A. (1998) Tunable Allignment of Macromolecules by filamentous phage yields dipolar coupling interactions. *Nat. Struct. Biol. 5*, 1065–1074.
26. Hansen, M. R., Hanson, P., and Pardi, A. (2000) Filamentous bacteriophage for aligning RNA, DNA, and proteins for measurement of nuclear magnetic resonance dipolar coupling interactions. *Methods Enzymol. 317*, 220–240.
27. Collaborative Computational Project Number 4 (1994) The CCP4 Suite: Programs for Protein Crystallography. *Acta Crystallogr. D50*, 760–763.
28. Tapia, M. I., Mourez, M., Hofnung, M., and Dassa, E. (1999) Structure-function study of MalF protein by random mutagenesis. *J. Bacteriol. 181*, 2267–2272.
29. Merino, G., Boos, W., Shuman, H. A., and Bohl, E. (1995) The inhibiton of maltose transport by the unliganded form of the

maltose-binding protein of *E. coli*: Experimental findings and mathematical treatment. *J. Theor. Biol. 177*, 171–179.
30. Dean, D. A., Hor, L. I., Shuman, H. A., and Nikaido, H. (1992) Interaction between Maltose-Binding Protein and the Membrane-associated Maltose Transporter Complex in *Escherichia coli*. *Mol. Microbiol. 6*, 2033–2040.
31. Manson, M. D., Boos, W., Bassford, P. J. J., and Rasmussen, B. A. (1985) Dependence of Maltose Transport and Chemotaxis on the Amount of Maltose-Binding Protein. *J. Biol. Chem. 260*, 9727–9733.
32. Austermuhle, M. I., Hall, J. A., Klug, C. S., and Davidson, A. L. (2004) Maltose-binding Protein Is Open in the Catalytic Transition State for ATP Hydrolysis during Maltose Transport. *J. Biol. Chem. 279*, 28243–28250.
33. Daus, M. L., Grote, M., and Schneider, E. (2009) The MalF-P2 loop of the ATP-binding cassette (ABC) transporter MalFGK2 from *Escherichia coli*/*Salmonella enterica* serovar Typhimurium interacts with maltose binding protein (MalE) throughout the catalytic cycle. *J. Bacteriol.* . doi: 10.1128/JB.01439-08.
34. Shilton, B. H., Shuman, H. A., and Mowbray, S. L. (1996) Crystal structures and solution conformations of a dominant-negative mutant of *E. coli* maltose-binding protein. *J. Mol. Biol. 264*, 364–376.
35. Davidson, A. L., and Chen, J. (2004) ATP-binding cassette transporters in bacteria. *Annu. Rev. Biochem. 73*, 241–268.

BI801376M